Measurement of D^0, D^+, D_s^+ and D^{*+} Production in Fixed Target 920 GeV Proton-Nucleus Collisions

I. Abt[24], M. Adams[11], M. Agari[14], H. Albrecht[13], A. Aleksandrov[30], V. Amaral[9], A. Amorim[9], S. J. Aplin[13], V. Aushev[17], Y. Bagaturia[13,37], V. Balagura[23], M. Bargiotti[6], O. Barsukova[12], J. Bastos[9], J. Batista[9], C. Bauer[14], Th. S. Bauer[1], A. Belkov[12,†], Ar. Belkov[12], I. Belotelov[12], A. Bertin[6], B. Bobchenko[23], M. Böcker[27], A. Bogatyrev[23], G. Bohm[30], M. Bräuer[14], M. Bruinsma[29,1], M. Bruschi[6], P. Buchholz[27], T. Buran[25], J. Carvalho[9], P. Conde[2,13], C. Cruse[11], M. Dam[10], K. M. Danielsen[25], M. Danilov[23], S. De Castro[6], H. Deppe[15], X. Dong[3], H. B. Dreis[15], V. Egorytchev[13], K. Ehret[11], F. Eisele[15], D. Emeliyanov[13], S. Essenov[23], L. Fabbri[6], P. Faccioli[6], M. Feuerstack-Raible[15], J. Flammer[13], B. Fominykh[23], M. Funcke[11], Ll. Garrido[2], A. Gellrich[30], B. Giacobbe[6], J. Gläß[21], D. Goloubkov[13,34], Y. Golubkov[13,35], A. Golutvin[23], I. Golutvin[12], I. Gorbounov[13,27], A. Gorišek[18], O. Gouchtchine[23], D. C. Goulart[8], S. Gradl[15], W. Gradl[15], F. Grimaldi[6], J. Groth-Jensen[10], Yu. Guilitsky[23,36], J. D. Hansen[10], J. M. Hernández[30], W. Hofmann[14], M. Hohlmann[13], T. Hott[15], W. Hulsbergen[1], U. Husemann[27], O. Igonkina[23], M. Ispiryan[16], T. Jagla[14], C. Jiang[3], H. Kapitza[13], S. Karabekyan[26], N. Karpenko[12], S. Keller[27], J. Kessler[15], F. Khasanov[23], Yu. Kiryushin[12], I. Kisel[24], E. Klinkby[10], K. T. Knöpfle[14], H. Kolanoski[5], S. Korpar[22,18], C. Krauss[15], P. Kreuzer[13,20], P. Križan[19,18], D. Krücker[5], S. Kupper[18], T. Kvaratskheliia[23], A. Lanyov[12], K. Lau[16], B. Lewendel[13], T. Lohse[5], B. Lomonosov[13,33], R. Männer[21], R. Mankel[30], S. Masciocchi[13], I. Massa[6], I. Matchikhilian[23], G. Medin[5], M. Medinnis[13], M. Mevius[13], A. Michetti[13], Yu. Mikhailov[23,36], R. Mizuk[23], R. Muresan[10], M. zur Nedden[5], M. Negodaev[13,33], M. Nörenberg[13], S. Nowak[30], M. T. Núñez Pardo de Vera[13], M. Ouchrif[29,1], F. Ould-Saada[25], C. Padilla[13], D. Peralta[2], R. Pernack[26], R. Pestotnik[18], B. AA. Petersen[10], M. Piccinini[6], M. A. Pleier[14], M. Poli[6,32], V. Popov[23], D. Pose[12,15], S. Prystupa[17], V. Pugatch[17], Y. Pylypchenko[25], J. Pyrlik[16], K. Reeves[14], D. Reßing[13], H. Rick[15], I. Riu[13], P. Robmann[31], I. Rostovtseva[23], V. Rybnikov[13], F. Sánchez[14], A. Sbrizzi[1], M. Schmelling[14], B. Schmidt[13], A. Schreiner[30], H. Schröder[26], U. Schwanke[30], A. J. Schwartz[8], A. S. Schwarz[13], B. Schwenninger[11], B. Schwingenheuer[14], F. Sciacca[14], N. Semprini-Cesari[6], S. Shuvalov[23,5], L. Silva[9], D. Škrk[18], L. Sözüer[13], S. Solunin[12], A. Somov[13], S. Somov[13,34], J. Spengler[13], R. Spighi[6], A. Spiridonov[30,23], A. Stanovnik[19,18], M. Starič[18], C. Stegmann[5], H. S. Subramania[16], M. Symalla[13,11], I. Tikhomirov[23], M. Titov[23], I. Tsakov[28], U. Uwer[15], C. van Eldik[13,11], Yu. Vassiliev[17], M. Villa[6], A. Vitale[6,7], I. Vukotic[5,30], H. Wahlberg[29], A. H. Walenta[27], M. Walter[30], J. J. Wang[4], D. Wegener[11], U. Werthenbach[27], H. Wolters[9], R. Wurth[13], A. Wurz[21], S. Xella-Hansen[10], Yu. Zaitsev[23], M. Zavertyaev[13,14,33], T. Zeuner[13,27], A. Zhelezov[23], Z. Zheng[3], R. Zimmermann[26], T. Živko[18], and A. Zoccoli[6]

[1] *NIKHEF, 1009 DB Amsterdam, The Netherlands* [a]
[2] *Department ECM, Faculty of Physics, University of Barcelona, E-08028 Barcelona, Spain* [b]
[3] *Institute for High Energy Physics, Beijing 100039, P.R. China*
[4] *Institute of Engineering Physics, Tsinghua University, Beijing 100084, P.R. China*
[5] *Institut für Physik, Humboldt-Universität zu Berlin, D-12489 Berlin, Germany* [c,d]
[6] *Dipartimento di Fisica dell' Università di Bologna and INFN Sezione di Bologna, I-40126 Bologna, Italy*
[7] *also from Fondazione Giuseppe Occhialini, I-61034 Fossombrone(Pesaro Urbino), Italy*
[8] *Department of Physics, University of Cincinnati, Cincinnati, Ohio 45221, USA* [e]
[9] *LIP Coimbra, P-3004-516 Coimbra, Portugal* [f]

[10] *Niels Bohr Institutet, DK 2100 Copenhagen, Denmark* [g]
[11] *Institut für Physik, Universität Dortmund, D-44221 Dortmund, Germany* [d]
[12] *Joint Institute for Nuclear Research Dubna, 141980 Dubna, Moscow region, Russia*
[13] *DESY, D-22603 Hamburg, Germany*
[14] *Max-Planck-Institut für Kernphysik, D-69117 Heidelberg, Germany* [d]
[15] *Physikalisches Institut, Universität Heidelberg, D-69120 Heidelberg, Germany* [d]
[16] *Department of Physics, University of Houston, Houston, TX 77204, USA* [e]
[17] *Institute for Nuclear Research, Ukrainian Academy of Science, 03680 Kiev, Ukraine* [h]
[18] *J. Stefan Institute, 1001 Ljubljana, Slovenia* [i]
[19] *University of Ljubljana, 1001 Ljubljana, Slovenia*
[20] *University of California, Los Angeles, CA 90024, USA* [j]
[21] *Lehrstuhl für Informatik V, Universität Mannheim, D-68131 Mannheim, Germany*
[22] *University of Maribor, 2000 Maribor, Slovenia*
[23] *Institute of Theoretical and Experimental Physics, 117218 Moscow, Russia* [k]
[24] *Max-Planck-Institut für Physik, Werner-Heisenberg-Institut, D-80805 München, Germany* [d]
[25] *Dept. of Physics, University of Oslo, N-0316 Oslo, Norway* [l]
[26] *Fachbereich Physik, Universität Rostock, D-18051 Rostock, Germany* [d]
[27] *Fachbereich Physik, Universität Siegen, D-57068 Siegen, Germany* [d]
[28] *Institute for Nuclear Research, INRNE-BAS, Sofia, Bulgaria*
[29] *Universiteit Utrecht/NIKHEF, 3584 CB Utrecht, The Netherlands* [a]
[30] *DESY, D-15738 Zeuthen, Germany*
[31] *Physik-Institut, Universität Zürich, CH-8057 Zürich, Switzerland* [m]
[32] *visitor from Dipartimento di Energetica dell' Università di Firenze and INFN Sezione di Bologna, Italy*
[33] *visitor from P.N. Lebedev Physical Institute, 117924 Moscow B-333, Russia*
[34] *visitor from Moscow Physical Engineering Institute, 115409 Moscow, Russia*
[35] *visitor from Moscow State University, 119992 Moscow, Russia*
[36] *visitor from Institute for High Energy Physics, Protvino, Russia*
[37] *visitor from High Energy Physics Institute, 380086 Tbilisi, Georgia*
[†] *deceased*

[a] supported by the Foundation for Fundamental Research on Matter (FOM), 3502 GA Utrecht, The Netherlands
[b] supported by the CICYT contract AEN99-0483
[c] supported by the German Research Foundation, Graduate College GRK 271/3
[d] supported by the Bundesministerium für Bildung und Forschung, FRG, under contract numbers 05-7BU35I, 05-7DO55P, 05-HB1HRA, 05-HB1KHA, 05-HB1PEA, 05-HB1PSA, 05-HB1VHA, 05-HB9HRA, 05-7HD15I, 05-7MP25I, 05-7SI75I
[e] supported by the U.S. Department of Energy (DOE)
[f] supported by the Portuguese Fundação para a Ciência e Tecnologia under the program POCTI
[g] supported by the Danish Natural Science Research Council
[h] supported by the National Academy of Science and the Ministry of Education and Science of Ukraine
[i] supported by the Ministry of Education, Science and Sport of the Republic of Slovenia under contracts number P1-135 and J1-6584-0106
[j] supported by the U.S. National Science Foundation Grant PHY-9986703
[k] supported by the Russian Ministry of Education and Science, grant SS-1722.2003.2, and the BMBF via the Max Planck Research Award
[l] supported by the Norwegian Research Council
[m] supported by the Swiss National Science Foundation

Abstract. The inclusive production cross sections of the charmed mesons D^0, D^+, D_s^+ and D^{*+} have been measured in interactions of 920 GeV protons on C, Ti, and W targets with the HERA-B detector at the HERA storage ring. Differential cross sections as a function of transverse momentum and Feynman's x variable are given for the central rapidity region and for transverse momenta up to $p_{\rm T} = 3.5$ GeV/c. The atomic mass number dependence and the leading to non-leading particle production asymmetries are presented as well.

1 Introduction

The cross sections for charm and beauty hadro-production are of considerable theoretical interest [1,2,3]. Perturbative QCD is expected to work well for the large mass top quark production and less well for the lower mass b and c quarks [1,2,3]. At present, several published results of measurements of charm production in proton-nucleus collisions [4,5,6,7,8,9] are available. They are mainly restricted to beam energies between 200 GeV and 800 GeV and mostly have low statistics. Only one of the experiments also provides a measurement of the dependence of the cross section on the atomic mass number. More data would help in determining the strong interaction parameters as well as in guiding the calculation of non-perturbative effects. Another motivation comes from the prediction that a prominent manifestation of the quark gluon plasma at the LHC is a larger ratio of charmonium to open charm cross section compared to, e.g., production in pA collisions at lower energies [10]. The present work provides a new data point at 920 GeV proton beam energy.

Collisions of the 920 GeV HERA proton beam in C, Ti and W fixed targets have been measured with the HERA-B spectrometer. In previous papers we have reported on the $b\overline{b}$ [11], Υ [12], and charmonium [13,14] production cross sections, while the present work deals with production of open charm in the inclusive reactions $pA \to DX$. Here D represents a D^0, D^+, D_s^+ or D^{*+} detected through the decay channels: $D^0 \to K^-\pi^+$, $D^+ \to K^-\pi^+\pi^+$, $D_s^+ \to \phi\pi^+ \to K^-K^+\pi^+$, and $D^{*+} \to D^0\pi^+ \to K^-\pi^+\pi^+$. Throughout this paper, charge-conjugated modes are included unless noted otherwise.

The paper is organized as follows. We first briefly describe the apparatus, the data sample and the method of analysis. We then present the results and finally make a comparison with other measurements and theoretical expectations.

2 The detector

HERA-B was a fixed target spectrometer (see Fig. 1) using the 920 GeV proton beam of the HERA *e-p* collider. Interactions occurred on one or more wires (depending on run configuration) which were organized into two groups of four target wires each; the groups were separated by 4 cm along the beam, and the transverse wire dimension was 50 μm-500 μm [15]. The wires were positioned in the beam halo, and their distance to the beam core was automatically adjusted to maintain a constant interaction rate. Details of the various subdetectors have been published [16,17,18,19,20,21], so only a brief overview of the apparatus is given here.

Tracks originating from proton interactions and decay vertices were measured with a vertex detector system (VDS) [16]. Sixty-four silicon strip detectors (50×70 mm^2, pitch of $\sim$50 μm) with double-sided readout were arranged in eight stations between 7 cm and 200 cm downstream of the targets. The detectors were in Roman pots [22] under vacuum and their inner edges were adjusted to be in the range 10-15 mm from the beam center. With this system, a vertex

Correspondence to: marko.staric@ijs.si

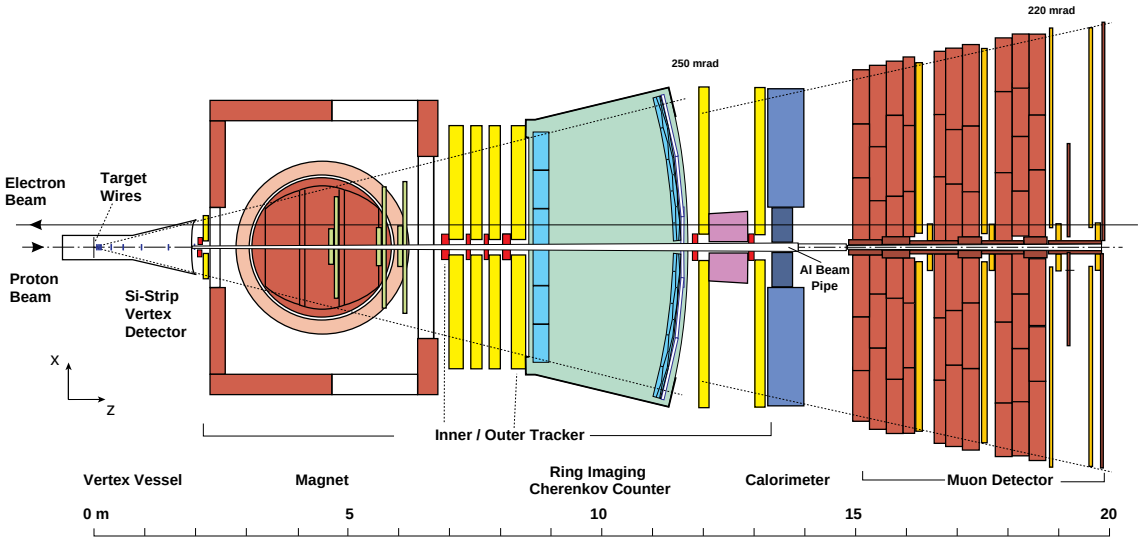

Fig. 1. A top view of the HERA-B detector.

resolution of $\sigma_z \sim 500$ μm along the beam direction and $\sigma_{x,y} \sim 50$ μm in the transverse plane was achieved.

Particle momenta were measured with a tracking system and a dipole magnet of 2.13 T·m field integral. The first tracking chamber was upstream of the magnet, and the remaining six chambers were downstream of the magnet between 7 m and 13 m from the interaction region. Due to a large variation of particle flux density, the tracking system was divided into a fine-grained inner tracker (ITR), using microstrip gas chambers with gas electron multipliers and $\sim$300 μm pitch [17], and a coarse-grained outer tracker (OTR), using honeycomb drift cells with 5 mm and 10 mm cell diameters [18]. The obtained momentum resolution can be parameterised as $\sigma_p/p = (1.61 + 0.0051 \cdot p\ [\mathrm{GeV}/c])$ % [18], where p is the particle momentum.

Particle identification was achieved with three subdetectors: a ring imaging Cherenkov counter (RICH), an electromagnetic calorimeter (ECAL), and muon chambers (MUON). The RICH detector [19] is a large vessel containing about 100 m^3 of C_4F_{10} gas at STP, which provided about 2 m of radiation path. The Cherenkov photons were focused and reflected by two sets of spherical and planar mirrors onto an upper and a lower photon detector, located well outside of the main particle flux. Each photon detector consisted of about 1100 multi-anode photomultiplier tubes. The identification efficiency for pions was about 90% in the momentum range from slightly above the pion threshold (2.4 GeV/c) up to 70 GeV/c, with the kaon misidentification probability always below 10%. The efficiency for kaons was above 85% for momenta between 15 GeV/c and 45 GeV/c, with a pion misidentification probability of $\sim$1%. For particles below the Cherenkov threshold of $\sim$10 GeV/c, the misidentification of pions as kaons was kept below 10%.

The ECAL [20] was a sampling calorimeter of the "shashlik" type, with scintillator plates sandwiched between tungsten (inner region) or lead (outer region) absorbers. The calorimeter was read out by optical fibers and photomultiplier tubes with the readout granularity of inner and outer regions adapted to different particle rates in order to maintain acceptable occupancies. The MUON system [21], situated in the most downstream region, consisted of four large detector stations separated by concrete and iron absorbers. Each muon detector plane had gas pixel chambers in the inner region and gas proportional tubes in the outer region.

For the present measurement, the analysis of data was based on the vertex detector, the OTR tracking system and the RICH counter.

Table 1. Summary of the data statistics and the integrated luminosities of the present study.

Target	A	events [$\times 10^6$]	$\mathcal{L}$ [μb^{-1}]
C	12.01	89.3	375
Ti	47.88	24.7	31
W	183.84	67.6	36

3 Data analysis

The analysis was performed on data sets with a single target wire made either of carbon, titanium or tungsten. Only runs with stable conditions and a minimum bias trigger were considered; the resulting sample consisted of 182 million interactions (Table 1). The trigger required at least 20 hits in the RICH detector (compared to an average of 33 for a full ring from a $\beta = 1$ particle [19]) and had an efficiency $\epsilon_{\rm trigger} \approx 95\%$ for inelastic interactions. The integrated luminosity $\mathcal{L}$ was determined [23] from the number of measured inelastic interactions $N_{\rm inel}$ and the total inelastic cross section $\sigma_{\rm inel}$, using the expression $\mathcal{L} = N_{\rm inel}/(\epsilon_{\rm trigger}\sigma_{\rm inel})$. The data were recorded at a moderate interaction rate of about 1.5 MHz which corresponds to 0.17 interactions per filled bunch crossing. Therefore only about 10% of triggered events contain more than one interaction. The data acquisition rate was about 1 kHz, and the bulk of the data was recorded within a two-week running period.

At the HERA-B energy, the charm production cross section is more than two orders of magnitude smaller than the inelastic cross section. Taking into account the relatively small branching ratios for the D meson decay modes into two or three charged particles, one expects sizeable backgrounds. Particle identification alone is not sufficient to extract signal events. However, the large boost of the center-of-mass system of HERA-B ($\gamma = 22$), causing D mesons to decay several millimeters from the target, combined with good vertex resolution ($\approx$0.5 mm longitudinally) allows us to distinguish D meson decay products from particles originating at the primary interaction point. The data selection thus requires a detached secondary vertex formed by tracks not coming from the primary interaction point as well as the identification of kaons and pions. The selection criteria are summarized in Table 2 and discussed in some detail below.

3.1 Data selection

In addition to a detached vertex for the ground state D mesons, at least one reconstructed primary vertex was required in each selected event. Primary vertices were determined from all track segments reconstructed in the VDS. Since the proton interaction point must be inside the target wire, the primary vertex coordinate transverse to the wire direction was replaced with the known target wire position.

For the tracks corresponding to the decay products of D mesons, mild requirements were applied on the number of hits in the vertex detector and in the main tracking system, as well as on the track fit quality. Selection criteria used to identify the final state kaons and pions were based on information from the RICH counter. While a rather strict cut on the kaon likelihood[1] was required for the kaon candidates ($L_K > 0.5$ for the D^0 and D^+ selection, and $L_K > 0.33$ for D_s^+ candidates), for pions only a mild cut was applied on the sum of RICH likelihoods for electrons, muons and pions, $L_e + L_\mu + L_\pi > 0.05$. No particle identification requirement was

[1] Likelihoods for the electron, muon, pion, kaon, proton and background hypotheses are normalized such that their sum is equal to one: $L_e + L_\mu + L_\pi + L_K + L_p + L_{\rm bkg} = 1$.

imposed for pions from $D^{*+} \to D^0\pi^+$ decays, which tend to have low momenta and are thus denoted as $\pi_{\rm slow}$.

The tracks were combined to form D^0, D^+ and D_s^+ candidates. Candidates with an invariant mass in the interval of ± 500 MeV/c^2 around the D meson nominal mass were retained for further analysis. For the D_s^+ candidates, the invariant mass of the K^+K^- pairs was required to be in the interval of ± 10 MeV/c^2 around the ϕ nominal mass; the absolute value of the cosine of the angle θ_ϕ between the K^+ and π^+ in the rest frame of the ϕ was restricted to the values above 0.5, exploiting the vector nature of the intermediate state ϕ. The D^{*+} candidates were reconstructed from D^0 candidates with invariant mass within ± 75 MeV/c^2 (3.5σ in resolution) of the D^0 mass and slow pion candidates, after a vertex fit to the D^0; an additional cut was applied on the product of transverse momenta of the D^0 daughter tracks and of the D^0 momentum, $p(D^0)p_{\rm T}(K)p_{\rm T}(\pi)$.

In addition to the criteria described above, the analysis was restricted to the region of phase space with high acceptance, $-0.15 < x_{\rm F} < 0.05$, where $x_{\rm F}$ is the Feynman x variable. The daughter tracks of a D meson candidate were fitted to a common vertex. Only combinations with a vertex probability greater than 0.1% and with a secondary vertex displaced by more than 4 standard deviations downstream of the wire were accepted.

The D meson candidate was then associated with the primary vertex. In the case of events with multiple reconstructed primary vertices, the vertex with the smallest impact parameter significance (i.e., the measured value divided by its estimated error given by the covariance matrix) with respect to the track of the D meson candidate was chosen. To avoid a possible bias in the primary vertex position due to tracks from the D meson candidate, the primary vertex was re-fitted without the D daughter tracks.

The final set of criteria was based on the primary and secondary vertices. The main source of background, which is due to combinations of particles emerging from the primary interaction point, was reduced by the following requirements: (1) the secondary vertex should be detached, (2) the tracks forming the secondary vertex should not come from the primary interaction point and (3) the D meson candidate should originate from the primary interaction point. To fulfill these criteria, cuts were applied on the following variables:

- $d(D)$ the significance of the distance between the secondary vertex and the associated primary vertex,
- $b(\pi), b(K)$ the significance of the impact parameter of a pion or kaon with respect to the primary vertex (in case more than one primary vertex was found, that closest to the particle is chosen),
- $b(D)$ the significance of the impact parameter of a D meson candidate with respect to the associated primary vertex.

We found that, for the three-body decays of D^+ and D_s^+, a more effective cut than a selection based on single impact parameter significances of daughter tracks is a cut on their product $b(K)b(\pi_1)b(\pi_2)$ and $b(K_1)b(K_2)b(\pi)$, respectively. The background level is further reduced with criteria of the form $\sqrt[3]{b(K)b(\pi_1)b(\pi_2)} > 4(t-t_0)$, for D^+, and $\sqrt{b(\phi)b(\pi)} > 0.75(t-t_0)$, for D_s^+. Here the proper lifetime t is in units of the D mean lifetime, and the offset t_0 is determined in an optimization.

For each decay mode the optimal cuts were determined by maximizing the signal significance $S/\sqrt{S+B}$ in a $\pm 3\sigma$ window centered at the D meson nominal mass (signal window). The signal S was taken from Monte Carlo simulation and was scaled to the luminosity of real data by using an estimation for the production cross sections from fits to the published D meson cross sections [1]. For the D_s^+ the cross section was assumed to amount to 20% of the sum of the D^0 and D^+ cross sections [2].

In the case of ground state D mesons, the number of background events B was estimated from the data sidebands. For the D_s^+, the mass region of ± 50 MeV/c^2 around the nominal mass of the D^+, where a contribution of the decay $D^+ \to \phi\pi^+$ is expected, was excluded from the lower sideband. To reduce the sensitivity to statistical fluctuations, the sidebands were chosen to be larger than the signal window. In the case of the D^{*+}, the wrong sign combinations from real data were used to estimate the background in the signal window. As is usually done for this decay, the signal was reconstructed via the mass difference $q = m(K,\pi,\pi_{\rm slow}) - m(K,\pi) - m_\pi$ rather than using the invariant mass of the $K,\pi,\pi_{\rm slow}$ combinations.

Table 2. Selection criteria; d and b denote decay distance and impact parameter significances, respectively, and L_h are likelihoods for a hypothesis h.

$D^0 \to K^-\pi^+$	$D^+ \to K^-\pi^+\pi^+$
chosen a priori	
$L_K(K) > 0.5$	$L_K(K) > 0.5$
$L_e(\pi) + L_\mu(\pi) + L_\pi(\pi) > 0.05$	$L_e(\pi) + L_\mu(\pi) + L_\pi(\pi) > 0.05$
optimized using background data and signal MC	
$d(D^0) > 6.1$	$b(D^+) < 2.6$
$b(D^0) < 2.4$	$b(K)b(\pi_1)b(\pi_2) > 106$
$b(K) > 3.4$	$\sqrt[3]{b(K)b(\pi_1)b(\pi_2)} > 4(t - t_0),\ t_0 = 2.48$
$b(\pi) > 3.7$	

$D_s^+ \to \phi\pi^+ \to K^-K^+\pi^+$	$D^{*+} \to D^0\pi^+ \to K^-\pi^+\pi^+$
chosen a priori	
$L_K(K) > 0.33$	$L_K(K) > 0.5$
$L_e(\pi) + L_\mu(\pi) + L_\pi(\pi) > 0.05$	$L_e(\pi) + L_\mu(\pi) + L_\pi(\pi) > 0.05$
$\lvert m(K^+K^-) - m(\phi)\rvert < 10$ MeV/c^2	$\lvert m(K\pi) - m(D^0)\rvert < 75$ MeV/c^2
$\lvert\cos(\theta_\phi)\rvert > 0.5$	$d(D^0) > 4$
optimized using background data and signal MC	
$d(D_s^+) > 5.3$	$b(D^0) < 2.4$
$b(D_s^+) < 2.11$	$b(K) > 2.1$
$b(K^-)b(K^+)b(\pi) > 28.7$	$b(\pi) > 1.7$
$\sqrt{b(\phi)b(\pi)} > 0.75(t - t_0),\ t_0 = 1.0$	$p(D^0)p_{\rm T}(K)p_{\rm T}(\pi) > 17.7(\text{GeV}/c)^3$

After applying the selection criteria, which are summarized in Table 2, the remaining data were scanned for events with more than one D meson candidate (in 0.5%, 8%, 0% and 20% of events for the D^0, D^+, D_s^+ and D^{*+} candidates, respectively). In case of the D^0, D^+ and D_s^+ candidates, the combinations with the largest decay distance significance $d(D)$ were kept. For the D^{*+} analysis, first the candidates whose intermediate D^0 had the largest decay distance significance were selected. If multiple candidates remained (i.e., due to multiple $\pi_{\rm slow}$ candidates), the D^{*+} candidate with the highest vertex probability was kept.

3.2 Signal yields

The invariant mass distributions for D meson candidates after applying the selection criteria discussed above are shown in Figs. 2-4.

The signal yields are extracted from the histograms by a maximum likelihood fit assuming Poisson statistics in individual bins. A Gaussian function is used for the signal, while the background description depends on the type of the D meson. For the D^+ and D_s^+, the background

is fitted by an exponential function. The background for D^0 candidates is more complex and consists of a combinatorial part, fitted by an exponential, and a contribution from partially reconstructed charm decays. This latter background is visible in the mass range below the D^0 peak. The shape of this background is taken from Monte Carlo simulation of $c\bar{c}$ events to which the same selection criteria are applied as for the data.

In the D_s^+ invariant mass distribution the Cabibbo suppressed decay of $D^+ \to \phi\pi^+$ is also seen (the peak to the left of the D_s^+ peak). This peak is included in the fit function as an additional Gaussian of the same width as the signal Gaussian, with its normalization as an additional free parameter, and its mean fixed to that extracted from the $D^+ \to K^-\pi^+\pi^+$ invariant mass distribution. The background for the D^{*+} candidates is parameterised as $a(q^{1/2} + bq^{3/2})$, with a and b as free parameters.

The fitted peak positions are within one standard deviation of the corresponding world average values [24], with the exception of D_s^+, which deviates by less than two standard deviations. The widths of the signal peaks are about 30% larger than the corresponding Monte Carlo values.

The numbers of reconstructed D mesons are summarized in Table 3. In total, 175 D^0, 131 D^+, 11 D_s^+ and 61 D^{*+} decays are found. The yields for various subsamples (particle, anti-particle, individual target material) are obtained by fitting with the mean and the width (r.m.s.) of the signal Gaussian function fixed to the values obtained from the fit to the full sample.

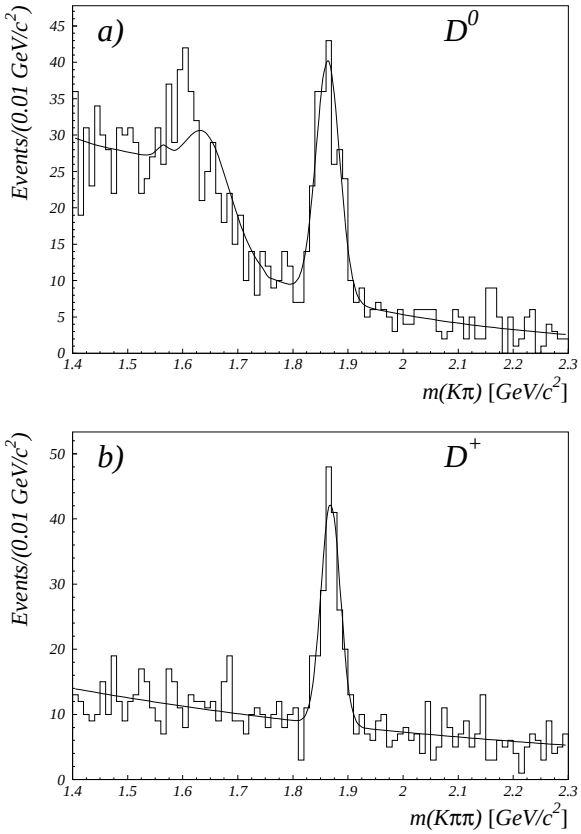

Fig. 2. Invariant mass distributions for $K^-\pi^+$ (a) and $K^-\pi^+\pi^+$ (b) combinations. The curves show results of maximum likelihood fits to the data.

The D meson proper time distributions provide a check for signal consistency. The acceptance-corrected distributions are found to be consistent with the expected exponential decay. To determine the lifetimes, a simultaneous likelihood fit of events in the signal window and in the

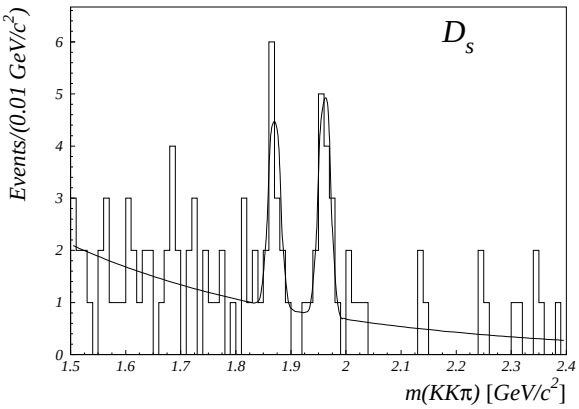

Fig. 3. Invariant mass distributions for $\phi\pi^+ \to (K^-K^+)\pi^+$ combinations. Besides the D_s^+ peak at 1.96 GeV/c^2, a D^+ peak at 1.87 GeV/c^2 is also visible. This peak corresponds to the Cabibbo suppressed decay $D^+ \to \phi\pi^+$. The curve shows the result of a maximum likelihood fit to the data.

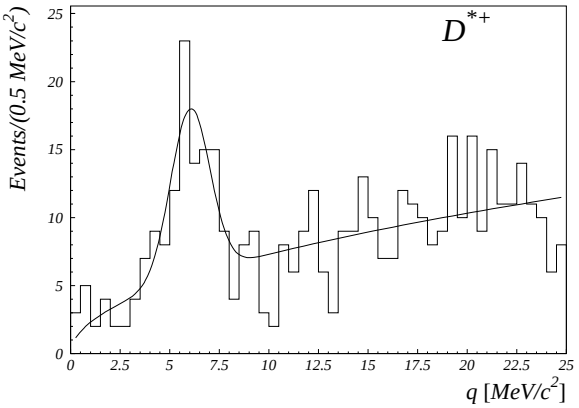

Fig. 4. Invariant mass difference $q = m(K,\pi,\pi_{\rm slow}) - m(K,\pi) - m_\pi$ for $K^-\pi^+\pi^+$ combinations. The curve shows the result of a maximum likelihood fit to the data.

Table 3. Number of reconstructed D mesons.

sample	D^0	D^+	D_s^+	D^{*+}
total	174.8±16.8	130.5±14.7	11.4±4.0	61.3±13.0
particle	75.9±10.9	54.5±9.3	4.9±2.6	21.0±6.6
anti-particle	99.0±11.9	75.8±10.5	6.7±2.8	40.6±8.3
C	66.1±9.6	43.1±7.7	4.2±2.2	26.6±6.4
W	92.3±11.7	72.4±10.6	6.7±3.0	24.8±7.5
Ti	17.4±5.7	14.9±5.0	0.4±1.0	9.6±4.0

sidebands is used. The results, $c\tau = (302\pm33)$ μm for D^+, (120±13) μm for D^0, and (165±52) μm for D_s^+, are in good agreement with the world average values [24].

As a further consistency check of the D_s^+ and D^{*+} signals, the intermediate states ϕ and D^0 are checked. They should be visible in the corresponding invariant mass distributions, when the signal region in the initial state invariant mass distribution is selected, and the fit to the intermediate state invariant mass distribution should give an event yield consistent with the number of events in the initial state peak. The yields extracted in this way are in good agreement with the values given in Table 3. For the D_s^+ decays, the distribution of the cosine of the angle between K^+ and π in the rest frame of the ϕ is found to be consistent with the expectation given by the vector nature of the intermediate state ϕ. The expected $D^+ \to \phi\pi^+$ signal yield

can be estimated from the number of reconstructed decays from our measured D^+ cross section in the $D^+ \to K^-\pi^+\pi^+$ decay channel. The fitted number of events, 9.8±3.8, is in reasonable agreement (1.4σ higher) with the estimated number, (4.2±1.2).

4 Efficiency determination

A Monte Carlo simulation is used to determine the signal reconstruction efficiencies. The Monte Carlo samples for $pA \to DX$ are generated in two steps. First, a $c\bar{c}$ pair is generated with Pythia 5.7 [25] such that a particular D meson is always produced. The generated events are re-weighted to make the resulting cross sections conform to the parameterisations

$$\frac{d\sigma}{dp_{\mathrm{T}}^2} \propto \left[1 + \left(\frac{\sqrt{\pi}\ \Gamma(\beta - \frac{3}{2})\ p_{\mathrm{T}}}{2\ \Gamma(\beta - 1)\ \langle p_{\mathrm{T}} \rangle}\right)^2\right]^{-\beta} \tag{1}$$

and

$$\frac{d\sigma}{dx_{\mathrm{F}}} = \begin{cases} A \exp\left(-\frac{x_{\mathrm{F}}^2}{2\sigma_g^2}\right)\ , |x_{\mathrm{F}}| < x_{\mathrm{b}}, \\ A'(1 - |x_{\mathrm{F}}|)^n\ , |x_{\mathrm{F}}| \geq x_{\mathrm{b}}, \end{cases} \tag{2}$$

with $\sigma_g = \sqrt{\frac{x_{\mathrm{b}}(1-x_{\mathrm{b}})}{n}}$ and $\ln \frac{A}{A'} = n[\frac{x_{\mathrm{b}}}{2(1-x_{\mathrm{b}})} + \ln(1-x_{\mathrm{b}})]$ [26]. The average transverse momentum of $\langle p_{\mathrm{T}} \rangle = 1.04 \pm 0.04$ GeV/c and the value of the exponent $\beta = 7.0 \pm 4.3$ are taken from the present analysis (Sec. 5.2). The value $n = 7.7 \pm 1.4$ is taken from the average of E743 and E653 [6,7], and x_{b} is assumed to be 0.062 ± 0.013 as measured by the E791 experiment [26]. The influence of the parameter uncertainties and other possible parameterisations of Eqs. 1 and 2 are taken into account as systematic errors. After the generation of the D mesons, the remaining energy is input to the Fritiof 7.02 [27] program package which generates the underlying event taking into account further interactions inside the nucleus.

The detector response is simulated with the Geant 3.21 package [28]. Realistic detector efficiencies, readout noise and dead channels are taken into account. The simulated events are processed by the same reconstruction codes used for the data.

5 Results

5.1 Total cross sections

The visible cross section per nucleus, i.e., the cross section measured in our visible range of $-0.15 < x_{\mathrm{F}} < 0.05$, is given by

$$\Delta\sigma_{\mathrm{pA},\,i} = \frac{N_i}{\mathrm{Br} \cdot \epsilon_i \cdot \mathcal{L}_i}, \tag{3}$$

where N_i is the number of reconstructed D mesons for a particular target i, ϵ_i and $\mathcal{L}_i$ are the corresponding efficiency and integrated luminosity, and Br is the world average branching ratio for a specific decay channel [24]. The cross section for D meson production on a nuclear target of atomic mass number A is parameterised as

$$\sigma_{\mathrm{pA}} = \sigma_{\mathrm{pN}} \cdot A^{\alpha}. \tag{4}$$

Table 4. Summary of systematic uncertainties of visible cross sections

Source	D^0	D^+	D_s^+	D^{*+}
Event fitting	3.4%	2.6%	6.0%	9.7%
Branching fractions	1.8%	3.6%	13.0%	1.9%
Luminosity	3.7%	3.7%	3.7%	3.7%
Reconstruction efficiency	8.4%	10.3%	12.9%	9.7%
Total	10%	12%	20%	14%

To combine data recorded with different target materials, the production cross sections per nucleon $\Delta\sigma_{\rm pN}$ are extracted in the following way. From Eq. 3 and Eq. 4, the D meson yield of the target i is derived,

$$N_i = {\rm Br} \cdot \epsilon_i \cdot \mathcal{L}_i \cdot \Delta\sigma_{\rm pN} \cdot A_i^{\alpha}. \tag{5}$$

By summing Eq. 5 over all targets and solving it for the production cross section we get

$$\Delta\sigma_{\rm pN} = \frac{N}{{\rm Br} \cdot \sum_i \epsilon_i \mathcal{L}_i A_i^{\alpha}}, \tag{6}$$

where $N = \sum_i N_i$ is the measured D meson yield of the total data sample. The sum in the denominator of Eq. 6 can be rewritten by introducing the average efficiency ϵ, defined by the weighted sum

$$\epsilon = \sum_i w_i \epsilon_i \quad , \qquad w_i = \frac{A_i^{\alpha}\mathcal{L}_i}{\sum_k A_k^{\alpha}\mathcal{L}_k}. \tag{7}$$

Then the expression 6 reads

$$\Delta\sigma_{\rm pN} = \frac{N}{{\rm Br} \cdot \epsilon \cdot \sum_i \mathcal{L}_i A_i^{\alpha}}. \tag{8}$$

Since there is no experimental indication for nuclear effects in open charm production, a linear A dependence of the cross sections is assumed, and α is set to one in Eqs. 7 and 8. This assumption is also in agreement with our measurements as discussed in Section 5.5.

The total systematic uncertainties are, according to Eq. 8, composed of contributions from uncertainty in the signal yields associated with the fitting procedure (listed as 'event fitting'), branching fractions, integrated luminosity and reconstruction efficiency. The uncertainty of the reconstruction efficiency can be further divided into contributions from Monte Carlo statistics, track reconstruction efficiency, particle identification efficiency, selection criteria and the contribution from the re-weighting of kinematical distributions based on $p_{\rm T}$ and $x_{\rm F}$. The individual contributions are summarized in Tables 4-5. The uncertainty due to selection criteria is determined in two ways: by varying the cut values in the selection criteria discussed above, and by performing a second analysis with an independent set of selection criteria. The change in the resulting cross section is taken as the corresponding systematic uncertainty. The systematic errors of track reconstruction and RICH particle identification (1.5% and 2.0% per track correspondingly) are estimated using decays of K_S^0 and ϕ as sources of pions and kaons. Note that no systematic error is assigned to the assumption $\alpha = 1$ in order to be compatible with previous experiments. Using Eq. 6 and data in Tables 1 and 6, $\Delta\sigma_{\rm pN}$ for $\alpha \neq 1$ can be extracted.

The resulting cross sections in the visible range, $\Delta\sigma_{\rm pN}$ and $\Delta\sigma_{\rm pA}$, are summarized in Tables 6-8. In order to extrapolate the measurements to the full phase space,

$$\sigma_{\rm pN} = \frac{\Delta\sigma_{\rm pN}}{f_{\rm vis}}, \tag{9}$$

Table 5. Summary of systematic uncertainties of reconstruction efficiency.

Source	D^0	D^+	D_s^+	D^{*+}
Monte Carlo statistics	1.2%	1.3%	3.7%	1.1%
Track reconstruction	3.0%	4.5%	4.5%	4.5%
Particle identification	4.0%	6.0%	6.0%	4.0%
Selection criteria	6.0%	6.0%	6.0%	6.0%
Re-weighting	2.9%	3.6%	7.7%	4.6%
Total	8.4%	10.3%	12.9%	9.7%

the fraction $f_{\rm vis}$ of D mesons in the visible range, defined by $-0.15 < x_{\rm F} < 0.05$, is determined in the following way. With the value of the exponent $n = 7.7 \pm 1.4$ as measured by the E743 and E653 experiments [6,7], $f_{\rm vis}$ is calculated by using Eq. 2. The values corresponding to the choice $x_{\rm b} = 0.062$ [26] and $x_{\rm b} = 0$ are 0.542±0.048 and 0.558±0.051, respectively. The difference is small compared to the uncertainty due to the error of the parameter n. For the extrapolation the average of both numbers, $f_{\rm vis} = 0.55 \pm 0.05$, is used. The resulting cross sections extrapolated to the full phase space are listed in Table 6.

Figure 5 shows the comparisons of these measured cross sections with other experimental studies. To compare the data points at different center-of-mass energies, the overall normalization of theoretical predictions given in [1] is determined separately for each of the D mesons by fits to the data which also include the results of the present measurements [2]. Our results are consistent with previous studies and represent an improvement at high energies. Note that our $\sigma(D^+)$ is somewhat lower than expected, leading to a lower ratio $\sigma(D^+)/\sigma(D^0)$ as will be discussed below.

The measured sum of the D meson cross sections per nucleon $\sigma(D^0) + \sigma(D^+) + \sigma(D_s^+) = (87.4 \pm 8.2 \pm 12.6)$ μb is used to determine the charm production cross section. From the fractions of charm hadrons produced in the hadronization of c quarks as measured in e^+e^- collisions, the

[2] The original measured values are rescaled in [1] by taking into account the updated D branching fractions. The result of $\sigma(D^0)$ by E789 is excluded from the fit.

Table 6. Cross sections in the visible range ($-0.15 < x_{\rm F} < 0.05$) and extrapolated to the full phase space. The first error is statistical and the second systematic. In the second column, the systematic error due to the extrapolation uncertainty is quoted separately.

	$\Delta\sigma_{\rm pN}[\mu{\rm b}]$ (visible range)	$\sigma_{\rm pN}[\mu{\rm b}]$ (full $x_{\rm F}$ range)
D^0	26.8±2.6±2.7	48.7±4.7±4.9±4.4
D^+	11.1±1.2±1.3	20.2±2.2±2.4±1.8
D_s^+	10.2±3.5±2.0	18.5±6.4±3.7±1.7
D^{*+}	11.9±2.6±1.7	21.6±4.7±3.0±2.0

Table 7. Cross sections for particle and anti-particle production in the visible range ($-0.15 < x_{\rm F} < 0.05$). The first error is statistical and the second systematic.

	$\Delta\sigma_{\rm pN}[\mu{\rm b}]$	
	particles	anti-particles
D^0	12.0±1.7±1.2	14.8±1.7±1.5
D^+	4.8±0.8±0.6	6.3±0.9±0.8
D_s^+	4.1±2.3±0.8	6.3±2.6±1.3
D^{*+}	4.5±1.4±0.6	7.2±1.5±1.0

Table 8. Visible cross sections per nucleus. Numbers in parentheses in the last row are for the subsamples of D^{*+} with D^0 daughters not common to the D^0 samples of the first row. The first error is statistical and the second systematic.

	$\Delta\sigma_{\rm pA}$ [mb]		
data sample	C	Ti	W
D^0	0.36± 0.05± 0.04	1.01± 0.33± 0.10	4.91± 0.62± 0.54
D^+	0.12± 0.02± 0.02	0.48± 0.16± 0.06	2.17± 0.32± 0.28
D_s^+	0.12± 0.07± 0.02	0.15± 0.35± 0.03	2.18± 0.99± 0.46
D^{*+}	0.17± 0.05± 0.03	0.71± 0.30± 0.10	1.71± 0.51± 0.26
	(0.21± 0.06± 0.03)	(0.95± 0.50± 0.14)	(2.11± 0.84± 0.34)

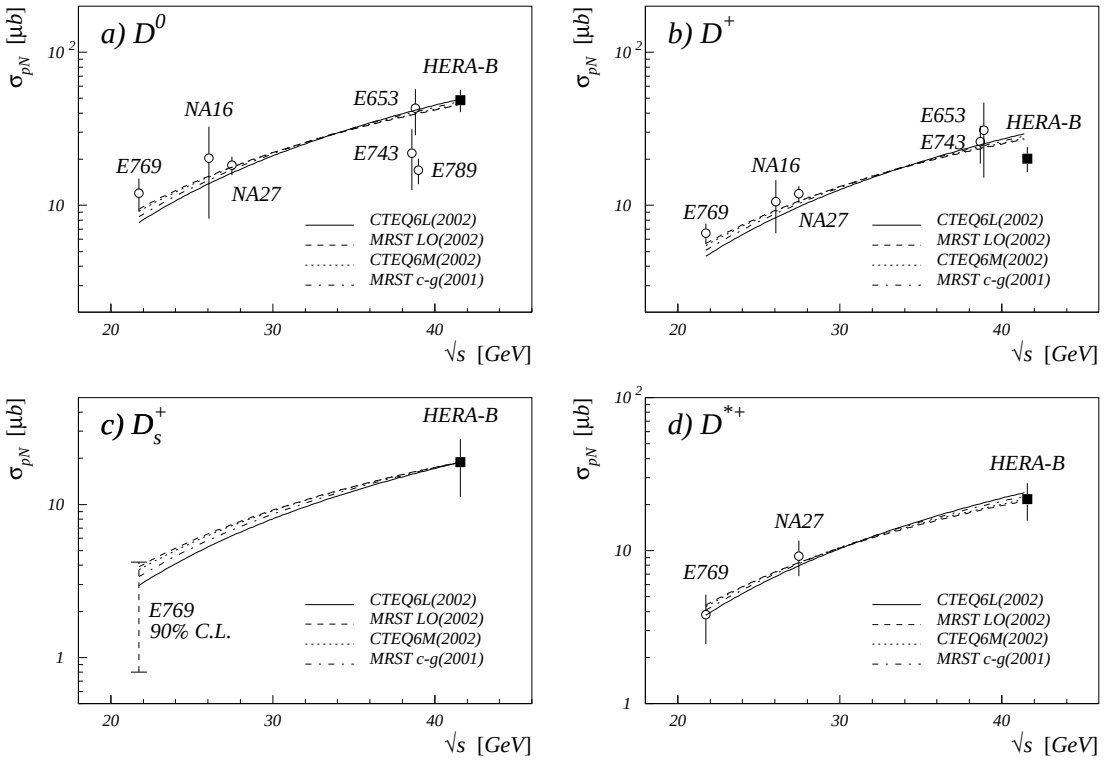

Fig. 5. Comparison of the present results with previous measurements [4,5,6,7,8,9]. In figure a) the result of E789 is excluded from the fit. The different curves correspond to different assumptions on parton distribution functions [1].

production of D^0, D^+ and D_s mesons is found to account for $f_D = 0.891 \pm 0.041$ of the charm cross section [29], where the uncertainty in f_D is obtained from errors in individual fractions neglecting possible correlations. Assuming the same fraction, the present study derives the charm cross section per nucleon, $\sigma(c\bar{c}) = (\sigma(D^0)+\sigma(D^+)+\sigma(D_s^+))/(2f_D)$, where the factor 2 accounts for the charge-conjugated states which are included in the D production cross sections. The resulting charm cross section per nucleon is thus $\sigma(c\bar{c}) = (49.1 \pm 4.6 \pm 7.4)$ μb. Note that due to correlations, the systematic error in the sum of cross sections is larger than the value which one would get by adding in quadrature the individual contributions.

5.2 Differential cross sections

The differential cross sections $d\sigma/dp_{\rm T}^2$ and $d\sigma/dx_{\rm F}$ are determined from production yields in bins of $p_{\rm T}^2$ and $x_{\rm F}$ by using Eq. 8. The yield in each individual bin is determined by subtracting from the number of events in the D meson signal window the number of background events as estimated from the sidebands. The resulting differential cross sections for the production of D^0 or D^+ mesons are shown in Fig. 6.

The parameters of the measured differential cross sections are determined in the following way. Because of the low statistics in individual bins of $p_{\rm T}^2$ and $x_{\rm F}$, we do not directly fit the background-subtracted distributions but instead do simultaneous binned likelihood fits of the $p_{\rm T}^2$ and $x_{\rm F}$ distributions of events in the mass signal and sideband windows. This correctly accounts for the Poisson errors.

For the transverse momentum distribution, several parameterisations can been found in the literature [2,26,30]. In the present analysis, the parameterisation given in Eq. 1 is used, since our previous studies of J/ψ, K^* and ϕ production indicate that it fits the data well over a large range of $p_{\rm T}^2$. The values of parameters $\langle p_{\rm T}\rangle$ and β are extracted from the fit. The distribution of background events $N_{\rm bgr}(p_{\rm T}^2)$ are assumed to be the same in shape and normalization for the signal window and sidebands. Several parameterisations of the distributions of events in sidebands fit well. We use the parameterization with two free parameters which gives the smallest χ^2/ndf: $Ce^{Bp_{\rm T}^2}$ for D^0 and D^+. The same parameterisation multiplied by the efficiency in $p_{\rm T}^2$, $Ce^{Bp_{\rm T}^2}\epsilon(p_{\rm T}^2)$, is used for D^{*+}.

The D^0, D^+ and D^{*+} data samples are fit simultaneously, where in the D^{*+} case only the subsample with D^0 daughters not common to the D^0 sample is included. The resulting fit parameters are $\langle p_{\rm T}\rangle = (1.04 \pm 0.04)$ GeV/c and $\beta = 7.0 \pm 4.3$, with χ^2/ndf=0.86. The measured $\langle p_{\rm T}\rangle$ is significantly larger (by 3.3σ) than the value extracted from the Pythia Monte Carlo samples (0.90 GeV/c), while β is, within one standard deviation, equal to the value extracted from the simulation ($\beta = 4.80$). Fitting with the fixed value of $\beta = 6$, i.e., the value used for our study of J/ψ production [13] yields the same $\langle p_{\rm T}\rangle$ value, and the same χ^2/ndf.

The $x_{\rm F}$ distribution is usually parameterised with a power-law function:

$$\frac{d\sigma}{dx_{\rm F}} \propto (1 - |x_{\rm F}|)^n. \tag{10}$$

This function differs in the central region from the predictions of the next-to-leading order QCD calculations [3]. The measurements made by E791 [26] in 500 GeV πA collisions using a high statistics sample of 80k reconstructed D^0 mesons also show a similar discrepancy. They obtain an improved fit with the function given in Eq. 2, which uses a power-law function in the tail region and a Gaussian in the central region[3].

In our analysis of the measured differential cross section $d\sigma/dx_{\rm F}$ (Fig. 6(b)), the boundary parameter $x_{\rm b}$ was fixed to the value $x_{\rm b} = 0.062$ as measured by E791 [26], because our range of $-0.15 < x_{\rm F} < 0.05$ is too small to determine this parameter. The exponent n, is extracted by simultaneously fitting the D^0 and D^+ data samples with a likelihood fit to the events in the signal windows and sidebands. While the fitted value of the exponent $n = 7.5 \pm 3.2$ agrees with the results of E653 [7] and E743 [6], the statistical error is larger in our study.

5.3 Ratios of cross sections

The measured cross section ratios are summarized in Table 9. The systematic errors come mainly from selection criteria, event fitting, branching fraction uncertainties and re-weighting, while the

[3] To account for the asymmetry in π-A collisions, E791 used an additional offset parameter

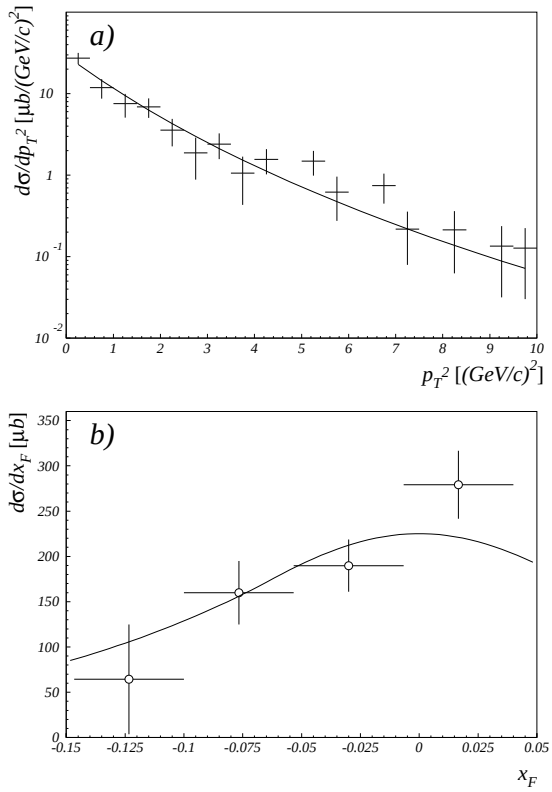

Fig. 6. Differential visible cross sections ($-0.15 < x_{\rm F} < 0.05$) for D^0 and D^+ production: (a) $d\sigma/dp_{\rm T}^2$, with the fit of Eq. 1, and (b) $d\sigma/dx_{\rm F}$ with the fit of Eq. 2 with a free parameter n and a fixed boundary parameter $x_{\rm b} = 0.062$.

Table 9. Ratios of cross sections. The first error is statistical and the second systematic.

D^+/D^0	0.41±0.06±0.04
D^{*+}/D^0	0.44±0.11±0.05
$D_s^+/(D^+ + D^0)$	0.27±0.09±0.05
D^{*+}/D^+	1.07±0.26±0.14

luminosity error cancels. The value for the ratio $\sigma(D^+)/\sigma(D^0) = 0.41 \pm 0.06 \pm 0.04$ is the most accurate measurement of this ratio in pA reactions. It is in good agreement with the combined results from hadroproduction [1] as well as from e^+e^- experiments [24]. The ratio also agrees with a simple prediction based on isospin symmetry and the measured ratio of vector to scalar meson production cross sections [1]. A comparison with results from other experimental studies is presented in Fig. 7.

The ratio $\sigma(D^{*+})/\sigma(D^0) = 0.44 \pm 0.11 \pm 0.05$ is also the most precise measurement of this ratio in pA reactions and is in good agreement with the results of NA27 and E769 [5, 9]. The vector to scalar meson production ratio $P_{\rm V}$ can be calculated in several ways (see [1] and references therein) if isospin invariance is assumed. From the ratio $R_1 = \sigma(D^+)/\sigma(D^0)$ one obtains $P_{\rm V} = (1 - R_1)/((1 + R_1){\rm Br}(D^{*+} \to D^0\pi^+)) = 0.61 \pm 0.09 \pm 0.06$. As a cross-check, we determine the same ratio from $R_2 = \sigma(D^{*+})/\sigma(D^+)$, and obtain the value $P_{\rm V} = R_2/(1 + {\rm Br}(D^{*+} \to D^0\pi^+) \cdot R_2) = 0.62 \pm 0.09 \pm 0.05$. The results are in good agreement with the world average value $P_{\rm V} = 0.59 \pm 0.01$ [1].

Our result for the ratio $\sigma(D_s^+)/(\sigma(D^0)+\sigma(D^+)) = 0.27 \pm 0.09 \pm 0.05$ is the first measurement of this quantity in pA reactions. For comparison, the world average value of measurements in e^+e^- collisions is 0.10±0.02 [24], and $0.112^{+0.024}_{-0.020}$ in deep inelastic scattering at HERA [31].

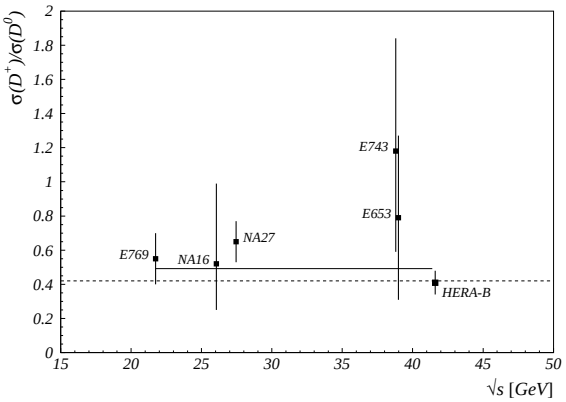

Fig. 7. Cross section ratio $R = \sigma(D^+)/\sigma(D^0)$, comparison with previous experiments. The dotted line at $R = 0.42$ shows the prediction of the isospin model with $P_V = 0.6$ [1]; the solid line is a fit to the data points.

Table 10. Leading to non-leading particle asymmetries $\mathcal{A}$ in the visible range, $-0.15 < x_F < 0.05$. The first error is statistical and the second systematic.

D^0	D^+	D^{*+}
0.10±0.09±0.05	0.14±0.11±0.06	0.23±0.17±0.06

5.4 Leading to non-leading particle asymmetries

A leading particle is defined as one which has a light quark in common with the beam particle, in our case: anti-D mesons $\overline{D}^0$, D^- and D^{*-}. The leading to non-leading particle asymmetry is defined as $\mathcal{A} \equiv (\sigma_{\rm LP} - \sigma_{\rm non\ LP})/(\sigma_{\rm LP} + \sigma_{\rm non\ LP})$. The measured values of the asymmetry in the visible range, $-0.15 < x_F < 0.05$, are given in Table 10 for the D^0, D^+ and D^{*+} mesons. The systematic uncertainty is dominated by the uncertainty of selection criteria and the kinematical re-weighting with respect to possible differences between leading and non-leading particles. Our measurements can be compared to the existing measurements of this asymmetry in different x_F intervals: by E769 (0.06±0.13, 0.18±0.11 and 0.36±0.26 for D^0, D^+ and D^{*+} mesons with $x_F > 0.0$ [9]), and E789 (0.02±0.06 for D^0 mesons with $0.0 < x_F < 0.08$ [8]).

5.5 Atomic mass number dependence

From the measured D meson production cross sections on three different target materials (Table 8), the exponent α of Eq. 4 can be determined. The results of simultaneous maximum likelihood fits to the invariant mass distributions of individual material data samples for each D meson are summarized in Table 11. The systematic error has two contributions: the uncertainty in the luminosity per wire material (about 2.2%), and Monte Carlo statistics (less than 1%). The observed value, $\alpha = 0.99 \pm 0.04 \pm 0.03$, is compatible with a linear dependence of the cross sections on atomic mass number ($\alpha = 1$). Note that for the weighted average of α over all four samples, only those D^{*+} events were considered for which the D^0 daughter particles were not reconstructed in the D^0 sample. Our result is in agreement with the result of E789 [8], $\alpha = 1.02 \pm 0.03 \pm 0.02$.

Table 11. Atomic mass number dependence parameter α and its weighted average for the four D mesons. For the weighted average the value in parenthesis of the fifth row were used, corresponding to the subsample of D^{*+} with D^0 daughter not common with the D^0 sample.

Particle	α
D^0	0.969±0.057±0.026
D^+	1.051±0.082±0.028
D_s^+	1.190±0.402±0.046
D^{*+}	0.832±0.138±0.022
	(0.847±0.185±0.022)
Average	0.994±0.044±0.025

6 Summary

With the HERA-B detector we have measured the total and single differential cross sections σ, $d\sigma/dp_{\rm T}^2$ and $d\sigma/dx_{\rm F}$, the atomic mass number dependence of the cross sections, and the leading to non-leading particle asymmetries for the production of D^0, D^+, D_s^+ and D^{*+} mesons in pA collisions at the proton energy of 920 GeV.

Extrapolating to the full phase space, the total cross sections per nucleon (in μb) are: $48.7 \pm 4.7 \pm 6.6$, $20.2 \pm 2.2 \pm 3.0$, $18.5 \pm 6.4 \pm 4.1$ and $21.6 \pm 4.7 \pm 3.6$ for the D^0, D^+, D_s^+ and D^{*+}, respectively. In the range $-0.15 < x_{\rm F} < 0.05$ the measured cross sections are: $26.8 \pm 2.6 \pm 2.7$, $11.1 \pm 1.2 \pm 1.3$, $10.2 \pm 3.5 \pm 2.0$ and $11.9 \pm 2.6 \pm 1.7$ for the D^0, D^+, D_s^+ and D^{*+}, respectively. The cross section per nucleon for $c\bar{c}$ production is $\sigma(c\bar{c}) = (49.1 \pm 4.6 \pm 7.4)$ μb.

We have measured the cross section ratios $\sigma(D^+)/\sigma(D^0) = 0.41 \pm 0.06 \pm 0.04$ and $\sigma(D^{*+})/\sigma(D^0) = 0.44 \pm 0.11 \pm 0.05$, as well as the vector to scalar meson production ratio, $P_{\rm V} = 0.61 \pm 0.09 \pm 0.06$. Our result for the ratio $\sigma(D_s^+)/(\sigma(D^0) + \sigma(D^+)) = 0.27 \pm 0.09 \pm 0.05$ is the first measurement of this quantity in pA reactions.

From the measured atomic mass number dependence of the production cross section, the parameter $\alpha = 0.99 \pm 0.04 \pm 0.03$ is extracted. This value is in agreement with the assumption of a linear dependence of cross sections, α=1. The measured leading to non-leading particle asymmetries in the $x_{\rm F}$ range $-0.15 < x_{\rm F} < 0.05$ are consistent with existing measurements for different $x_{\rm F}$ regions.

The results of our studies are in good agreement with previous measurements of open charm production in pA interactions and provide, in the majority of cases, an improvement in accuracy.

Acknowledgments

We express our gratitude to the DESY laboratory for the strong support in setting up and running the HERA-B experiment. We are also indebted to the DESY accelerator group for their continuous efforts to provide good and stable beam conditions. The HERA-B experiment would not have been possible without the enormous effort and commitment of our technical and administrative staff. It is a pleasure to thank all of them.

References

1. C. Lourenço, H.K. Wöhri, Phys. Rept. **433**, 127 (2006)
2. S. Frixione, M.L. Mangano, P. Nason, G. Ridolfi, Adv. Ser. Direct. High Energy Phys. **15**, 609 (1998)
3. P. Nason, S. Dawson, R.K. Ellis, Nucl. Phys. **B327**, 49 (1989) (Erratum-ibid. **B335**, 260 (1990))
4. M. Aguilar-Benitez et al. (NA16 Collaboration), Phys. Lett. B **135**, 237 (1984)
5. M. Aguilar-Benitez et al. (NA27 Collaboration), Z. Phys. C **40**, 321 (1988)

6. R. Ammar et al. (E743 Collaboration), Phys. Rev. Lett. **61**, 2185 (1988)
7. K. Kodama et al. (E653 Collaboration), Phys. Lett. B **263**, 573 (1991)
8. M.J. Leitch et al. (E789 Collaboration), Phys. Rev. Lett. **72**, 2542 (1994)
9. G.A. Alves et al. (E769 Collaboration), Phys. Rev. Lett. **77**, 2388 (1996) (Erratum-ibid. **81**, 1537 (1998))
10. A. Andronic, P. Braun-Munziger, K. Redlich, J. Stachel, Phys. Lett. B **571**, 36 (2003); Nucl. Phys. A **789**, 334 (2007)
11. I. Abt et al. (HERA-B Collaboration), Phys. Rev. D **73**, 052005 (2006)
12. I. Abt et al. (HERA-B Collaboration), Phys. Lett. B **638**, 13 (2006)
13. I. Abt et al. (HERA-B Collaboration), Phys. Lett. B **638**, 407 (2006)
14. I. Abt et al. (HERA-B Collaboration), Eur. J. Phys. C **49**, 545 (2007)
15. K. Ehret, Nucl. Instrum. Methods A **446**, 190 (2000)
16. C. Bauer et al., Nucl. Instrum. Methods A **501**, 39 (2003)
17. W. Gradl, Nucl. Instrum. Methods A **461**, 80 (2001)
18. H. Albrecht et al., Nucl. Instrum. Methods A **555**, 310 (2005); ibid. A **541**, 610 (2005); ibid. A **576**, 312 (2007)
19. I. Ariño et al., Nucl. Instrum. Methods A **516**, 445 (2004)
20. G. Avoni et al., Nucl. Instrum. Methods A **461**, 332 (2001)
21. V. Eiges et al., Nucl. Instrum. Methods A **461**, 104 (2001)
22. R. Battiston et al., Nucl. Instrum. Methods A **238**, 35 (1985)
23. I. Abt et al. (HERA-B Collaboration), arXiv:0706.0131 [physics.data-an] (2007)
24. W.-M. Yao et al. (Particle Data Group), J. Phys. G: Nucl. Part. Phys. **33**, 1 (2006)
25. T. Sjöstrand, Comp. Phys. Commun. **82**, 74 (1994)
26. E.M. Aitala et al. (E791 Collaboration), Phys. Lett. B **462**, 225 (1999)
27. H. Pi, Comp. Phys. Commun. **71**, 173 (1992)
28. R. Brun et al., GEANT3 (Internal Report CERN-DD/EE/84-1, CERN) (1987)
29. W.-M. Yao et al. (Particle Data Group), J. Phys. G: Nucl. Part. Phys. **33**, 200 (2006)
30. G.A. Alves et al. (E769 Collaboration), Phys. Rev. Lett. **77**, 2392 (1996)
31. S. Chekanov et al. (ZEUS Collaboration), arXiv:0704.3562 [hep-ex] (2007)